

Journal of Materials Chemistry A

Accepted Manuscript



This is an *Accepted Manuscript*, which has been through the Royal Society of Chemistry peer review process and has been accepted for publication.

Accepted Manuscripts are published online shortly after acceptance, before technical editing, formatting and proof reading. Using this free service, authors can make their results available to the community, in citable form, before we publish the edited article. We will replace this *Accepted Manuscript* with the edited and formatted *Advance Article* as soon as it is available.

You can find more information about *Accepted Manuscripts* in the [Information for Authors](#).

Please note that technical editing may introduce minor changes to the text and/or graphics, which may alter content. The journal's standard [Terms & Conditions](#) and the [Ethical guidelines](#) still apply. In no event shall the Royal Society of Chemistry be held responsible for any errors or omissions in this *Accepted Manuscript* or any consequences arising from the use of any information it contains.

Remarkable Capacitive Behavior of Co_3O_4 -Polyindole Composite as Electrode Material for Supercapacitor Applications

R. Pavul Raj^a, P. Ragupathy^{*b}, S. Mohan^{*a}

^aElectroplating and Metal Finishing Technology Division,

^bFuel Cells Section, Electrochemical Power Sources Division,

CSIR - Central Electrochemical Research Institute,

Karaikudi-630003, India.

Keywords: Cathodic polymerization; Co_3O_4 -Polyindole composites; Supercapacitor; rate capability.

* To whom all correspondence should be addressed,

E-mail: mohan40159@cecri.res.in and ragupathyp@cecri.res.in

Tel: +91 04565 241261, +91 04565 241361

Abstract

In this paper, we demonstrate a single step synthesis of Cobalt oxide – conducting Polyindole (Co₃O₄-Pind) composites by *in-situ* cathodic electrodeposition. The structural and morphological changes of as prepared Co₃O₄-Pind composites have been investigated using various techniques such as powder X-ray diffraction (XRD), scanning electron microscopy (SEM), transmission electron microscopy (TEM), Raman analysis and X-ray photoelectron spectroscopy (XPS). Very interestingly, polyindole decoration over Co₃O₄ results a concomitant change in the morphology having substantial improvement in the supercapacitor behavior. The electrochemical performance of Co₃O₄-Pind has been carried out using cyclic voltammetry, galvanostatic charge-discharge cycling and impedance analysis. The specific capacitance (SC) of Pind decorated Co₃O₄ is found to be 1805 Fg⁻¹ at a current density of 2 Ag⁻¹ with excellent rate capability (SC: 1625 Fg⁻¹ at a high current density of 25 Ag⁻¹) and cycling stability. This remarkable supercapacitive performance of Co₃O₄-Pind composite is mainly attributed to the synergism evolved between Co₃O₄ and Pind. More importantly, these electrodes are free from binders and conductive carbon which has significant impact over the gravimetric energy density of the devices.

Introduction

Ever increasing energy demand, depletion of fossil fuels and global warming have urged the researchers to develop green and sustainable energy storage systems.¹⁻⁵ Among various energy storage systems, supercapacitor is believed as one of the most promising candidate due to its high power density, fast charge-discharge process, long cycle life and environmentally benign. More importantly, supercapacitors possess higher power density than Li ion batteries and higher energy density than conventional dielectric capacitors occupying the region between batteries/fuel cells and capacitors in the Ragone plot.⁶ The energy storage mechanism of supercapacitors is classified into two categories namely double layer capacitor in which charge accumulates at electrode/electrolyte interface and pseudocapacitors wherein charge storage is due to mainly Faradaic process. The various carbon, transition metal oxides/hydroxides and conducting polymer have been widely used as active materials for supercapacitors.^{4,7-9} Among the various materials investigated over the years, transition metal oxides are attractive due to their chemical stability, variable valence etc.,¹⁰ Particularly, Cobalt oxide has been considered as most appealing candidate for supercapacitors because of its high theoretical SC (3560 Fg^{-1}), reversibility¹¹ and superior electrochemical performance.¹² Variety of cobalt oxide nanostructures have been prepared using different routes like hydrothermal,¹³⁻¹⁷ calcination,¹⁸ electrospinning,¹⁹ electrodeposition²⁰⁻²³ etc., For instance, ultralayered Co_3O_4 structures have been synthesized by Rao et.al exhibiting SC of 548 Fg^{-1} at a current density of 8 Ag^{-1} with reasonable cycling stability.²⁴ Y. Wang et.al have prepared 3D-nanonet hollow structured Co_3O_4 which offers high SC of 820 Fg^{-1} at scan rate of 5 mVs^{-1} .¹⁸ Similarly, controlled morphology of nanoporous Co_3O_4 obtained using a simple solvothermal exhibits the specific capacitance, energy density and power density of 476 Fg^{-1} , 42.3 Wh kg^{-1} and 1.56 kW kg^{-1} respectively.²⁵ However,

the poor electronic conductivity, limited SC and poor electrochemical stability during cycling are prone for Co_3O_4 similar to other transition metal oxides. To overcome these drawbacks, the nanostructured Co_3O_4 are assembled with carbon matrix to form composites. Such combination of metal oxide and carbon is a promising approach to control, develop, and design high performance active materials for supercapacitors.²⁶ Accordingly, various hybrid materials such as Co_3O_4 /graphene,^{5,27} Co_3O_4 /carbon nanotube (CNT),²⁸ and Co_3O_4 /carbon nanofibers (CNF)¹⁹ with enhanced electrical conductivity and large surface area providing efficient contact between active materials and electrolyte. However, designing a single step process to prepare Co_3O_4 / carbon with improved supercapacitive behavior has not been reported. Moreover, there is no report on Co_3O_4 / polymer obtained by electrodeposition for supercapacitor studies. Recently, conducting polymers receives much interest as they provide high pseudocapacitance value due to redox behavior and fast charge discharge process.²⁹ Particularly, Polyindole (Pind) has attracted considerable interest due to the combinational properties of both poly(p-phenylene) and polypyrrole together, such as fairly good thermal stability, high redox property, slow degradation and better air stability³⁰ compared with polypyrrole and polyaniline.³¹ The combination of conducting polymers and metal oxides would provide enhanced electrochemical performance in energy storage devices due synergism between them.³ Thus, much attention has been paid to produce metal oxides embedded in conducting polymer matrix which eventually increases the conductivity of electrodes greatly improving the SC value, rate capability and cycling stability. For instance, Yongju Jung et.al.,³²⁻³⁴ have notified a new synthesis strategy that enables cathodic deposition of conducting polymers by utilizing cathodically generated oxidizing agents for oxidative chemical polymerization of conducting polymers. However, the reports available on the preparation of metal oxides-polymer composites especially for supercapacitor applications

are scarce in the literature. In this paper, we report a simple and single step synthesis of Co₃O₄-Pind composites involving cathodic conducting polymerization and electrodeposition. Moreover, utilization of Co₃O₄-Pind composites without binder and conductive carbon as electrode material for supercapacitor offers remarkable SC and rate capability.

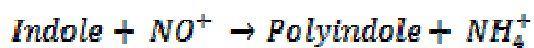
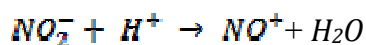
Experimental section

Materials

Sodium Nitrate (NaNO₃), Nitric acid (HNO₃), Cobalt Nitrate (Co(NO₃)₂), Indole, Graphite sheet and stainless steel (SS 304) were purchased from Alfa Aesar, India and used without further purification.

Preparation of Co₃O₄ – Pind composite electrode

An aqueous solution containing 0.25 M NaNO₃, 0.05 M Co(NO₃)₂ and 0.01 M HNO₃ was used as an electrolyte for Co₃O₄ deposition. To obtain Co₃O₄-Pind composites, 0.01 M indole monomer was added to the above electrolyte. Also, the solubility of indole monomer in aqueous solution was ensured by warming the solution at 60°C for few mins. The SS 304 foil and graphite sheet were used as cathode and anode respectively. The deposition of oxides and composites were carried out by galvanostatic method. The current densities of 450 and 700 mAcm⁻² were applied for 3 mins to obtain Co₃O₄ and Co₃O₄-Pind composites respectively. For comparison study, bare Pind was also prepared with the similar deposition condition without Co(NO₃)₂. The following reactions are evidenced for the cathodic polymerization process³²⁻³⁴.



Physical and electrochemical characterization

Morphology and structural characterization of Co_3O_4 and Co_3O_4 -Pind composites were studied using powder X-ray diffraction (XRD) (PANalytical X'pert pro), infrared (FTIR) (BRUKER - TENSOR 27), laser Raman (Renishaw Invia Raman Spectroscopy and Microscope) spectroscopy, scanning electron microscopy (SEM) (Vega-3 TESCA) transmission electron microscopy (TEM), (FEI-Tecanai 20 G2) and X-ray photoelectron spectroscopy (XPS) (Thermo Scientific - MULTILAB 2000). The cyclic voltammetry, charge discharge cycling and impedance analysis were carried out using potentiostat (Solartron model-1470E), in 1 M KOH solution using three electrode configuration. The electrodeposited (Co_3O_4 , Co_3O_4 -Pind composites and Pind), platinum (Pt) foil and Ag/AgCl were employed as working, counter and reference electrodes respectively. The SC was calculated using the galvanostatic charge-discharge curves according to formula:

$$\text{SC} = I t / (m \Delta E) \quad (1)$$

where I is current in Ampere (A) used for charge-discharge cycling, t is the time in seconds (s) of discharge, m is the mass in grams of the active material and ΔE is the operating potential window in volt (V) of charge or discharge

Results and discussion

Structural characterization

Figure 1 shows the powder XRD patterns of pristine Co_3O_4 and Co_3O_4 -Pind composites. Accordingly, all observed reflections found in Figure 1(i) could be indexed to cubic structure (JCPDS No. 00-073-1701) with Fd-3m (227) space group of Co_3O_4 . There was no characteristic peaks of any impurity were observed indicating the high quality oxides. Figure 1(iii) shows broad diffraction angle indicating the amorphous nature of the polymer (Molecular formula:

$C_8H_6N-(C_8H_5N)_n-C_8H_6N$). Apparently, Figure 1(ii) shows broad peaks around 25 and 34° values clearly indicating the existence of Pind as also evidenced from IR analysis.

Raman spectroscopy is an extremely useful tool to study the structural features of materials. Accordingly, Figure 2(a) shows superimposed Raman spectra of pristine Co_3O_4 , Co_3O_4 -Pind and Pind. As seen in Figure 2(a) (i), a broad peak at 950 cm^{-1} Raman shift is mainly attributed to O-Co-O bending. Two more board peaks (525 and 630 cm^{-1}) and one strong peak (600 cm^{-1}) are strong evident for spinel structure of cobalt oxide deposited on SS foil.^{35,36} Polyindole aromatic characteristic asymmetry and symmetric stretching peaks are observed at 1700 and 1614 cm^{-1} respectively as shown Figure 2(a) (iii). The peaks observed at 1367 and 1331 cm^{-1} are due to ring stretching frequency, while the peaks at 1235 and 1107 cm^{-1} correspond to out-of-plane and in-plane deformation of N-H, while the peaks 1001 and 932 cm^{-1} peaks are out-of-plane and in-plane deformation of C-H.³⁷ Simply, the peaks observed for Co_3O_4 -Pind composite are possibly due to synergetic peaks of Pind and Co_3O_4 . A peak at 600 cm^{-1} indicates the defected Co_3O_4 -Pind spinel structure confirming by tetrahedral Co-O bending frequency³⁶ as seen in Figure 2(a) (ii).

Figure 2(b) shows the compared IR spectra of Co_3O_4 and Co_3O_4 -Pind. A broad peak observed at 630 cm^{-1} is assigned to metal-oxygen bending vibration (Figure 2(b) (i)). The strong peaks observed at 1428 and 1347 cm^{-1} as seen in Figure 2(b) (ii) are mainly attributed to asymmetry and symmetry stretching frequency of $-C=N$ respectively. It is notified that there is small peak at 1306 cm^{-1} revealing week binding of metal oxide stretching frequency.³⁸ The stretching frequency of $-C-C=N$ is seen at 1039 cm^{-1} and similarly strong and broad peak of $-NH$ wagging are observed in 632 cm^{-1} . The $-CH$ out of plane bending frequency is shown in 496 cm^{-1} . In Figure 2(b) (iii), the absorption peaks of Pind at 1611 and 1451 cm^{-1} doublet peaks

correspond to the bending mode of aromatic alkene and –NH bending vibration mode respectively. The peaks observed at 1351 cm^{-1} and 1243 cm^{-1} are due to stretching vibration mode of C-N and C-C respectively. The symmetric and asymmetric bending modes of aromatic hydrogen in out of plane bending are detected at 1089 and 1012 cm^{-1} . A peak at 747 cm^{-1} resembles the bending mode of benzene ring. The NH wagging absorption bands are due to the peaks at 610 and 505 cm^{-1} .^{39,40} These physicochemical characterizations are evidence for the formation of Co_3O_4 -Pind composite.

X-ray photo electron spectroscopy is a useful tool to understand variation in the oxidation state and degree of functionalization. Accordingly, Figure 3(a) shows the deconvoluted XPS spectra of Co indicating the spin orbit coupling of Co $2p_{3/2}$ and Co $2p_{1/2}$. The peaks observed at 779.7 and 795.77 eV are evident for the Co_3O_4 of Co $2p_{3/2}$ and Co $2p_{1/2}$ in the composites. The peak difference between Co $2p_{3/2}$ and $2p_{1/2}$ is 15.7 eV . It almost matches with standard spin orbit coupling of Co $2p_{3/2}$ and Co $2p_{1/2}$. The BE values of Co_3O_4 -Pind composites are observed at 783.47 , 785.75 , 801.07 and 803.39 eV with low intense peaks indicating the mixed valence of Co (Co^{2+} and Co^{3+}).^{36,41} Remaining peaks at 781.41 , 797.59 and 807 eV are indicating the interaction of Cobalt and electronegative elements. Figure 3(b) shows the XPS spectra of C1s of Co_3O_4 –Pind composites. The aromatic sp^2 type Carbon is observed at 284.1 eV and the peaks 285.71 and 284.79 eV are assigned to C=N, C-N respectively. The characteristic aromatic satellite peak is indicated at 287.6 eV .⁴² Figure 3 (c) shows the pyrolytic type nitrogen peak is observed at 399.62 eV . An interaction of Cobalt and Nitrogen is evident from a peak obtained at 399.74 eV . The –C-N and –C=N peaks are observed at 399 and 400.43 eV respectively. The deconvoluted O1s spectrum is shown in Figure 3(d) which indicates the existence of four

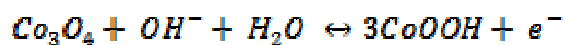
different oxygen species. The BE values at 529.58, 530.27, 531.06 and 532.13 eV are mainly attributed to Co-O, -OOH, -OH and H-O-H respectively.⁴³⁻⁴⁵

Microscopic analysis

In order to understand the surface morphology and microstructure of the as-prepared Pind, Co₃O₄ and Co₃O₄-Pind composites, scanning electron microscopy (SEM) analysis were performed. Accordingly, Figure 4(a-c) shows the SEM images of pristine Co₃O₄, pristine Pind, and Co₃O₄-Pind composites respectively. It is seen that Co₃O₄ deposited on SS forms as bundles of nanorods with length of 0.5-1.0 μm (Figure. 4(a)) and diameter of 200-300 nm. In the case of Pind, homogenously well distributed porous sponge like morphology is obtained as shown in Figure 4(b). Very interestingly, while the formation of Co₃O₄-Pind composite, rods and sponge like structures of Co₃O₄ and Pind respectively, are converted in to well distributed particles with the size ranging from 200 nm to 800 nm as shown in Figure 4(c). Furthermore, the EDX images confirmed the presence of Co, Indole composition in Co₃O₄-Pind composite along with bare SS substrate (304 grade). Further insights about crystallographic information the transmission electron microscope images were recorded. Typical TEM image of Co₃O₄-Pind is shown in Figure 5. The dark contrast portion is evident for an interesting feature of the oxide particles embedded on polymer as indicated in the Figure 5 (a). Further, Figure 5 (b) depicts the selected area electron diffraction (SAED) pattern having the d spacing value of 1.56 Å and 1.45 Å which correspond to (511) and (440) planes respectively. This result is consistent with powder XRD analysis.

Electrochemical analysis

With an aim to understand the supercapacitive behavior of Co₃O₄-Pind composite, cyclic voltammetry (CV) and galvanostatic charge–discharge (GCD) curves were recorded in a potential range between -0.2 and 0.5 V in 1 M KOH. Accordingly, a comparative study of cyclic voltammograms of pristine Co₃O₄, Co₃O₄-Pind composite and Pind is shown in Figure 6(a). It can be seen from CV curves (Figure 6(a)) that characteristic redox peaks (0.15 V and 0.1 V) are mainly attributed to the Faradaic reaction of Co₃O₄.^{46–49} The reactions are presented as follows.



On the other hand, CV of Co₃O₄-Pind composite also exhibits the redox peaks corresponding to Faradaic process similar to pristine Co₃O₄. However, it is observed that there is shift in the peak position and asymmetry nature of anodic and cathodic peak indicating the significant impact of Pind in Co₃O₄ in the redox process. Furthermore, the variation in the double layer current is notified between Co₃O₄ and Co₃O₄-Pind composite demonstrating the combination of double layer and Faradaic pseudocapacitance which contributes enhanced the SC of Co₃O₄-Pind composite electrodes. Further, the large potential difference between anodic and cathodic peaks in Co₃O₄-Pind composite compared to that of pristine Co₃O₄ is believed to have significant impact on not only the rate performance but also in the double layer capacitance.

In order to understand the reversibility of the composites electrodes, CVs were recorded at different scan rates in the range 1-100 mVs⁻¹ and the corresponding data is shown in Figure 6 (b). The peak current increases with an increase in the scan rate illustrating its good reversibility during the fast charge–discharge process. Additionally, the increased potential difference

between anodic and cathodic peaks is mainly attributed to the polarization of the electrode under a high scan rate. As the scan rate increases, anodic peaks shift to a higher potential and cathodic peaks shift to a lower potential that clearly reveals the limitation of the ion diffusion rate to satisfy electronic neutralization during the redox reaction. Similar observations are made earlier for such oxides.^{17,18}

Table 1 A comparison of various Co_3O_4 and its composites materials for Supercapacitors.

Material	Preparation Method	Specific Capacitance	Current Density	Electrolyte	Cycle Performance	Ref.
Cobalt oxide	Electrodeposition	235 Fg^{-1}	20 mVs^{-1}	2 M KOH	Not mentioned	50
Hierarchically Co_3O_4 film	Electrodeposition	443 Fg^{-1}	2 Ag^{-1}	2 M KOH	Hierarchical structure maintains after 3000 cycles	51
		334 Fg^{-1}	40 Ag^{-1}			
Co_3O_4 nanosheets	Electrodeposition	1033.3 Fg^{-1}	2.5 Ag^{-1}	5 M KOH	77% retention after 3000 cycles	23
$\text{Co}_3\text{O}_4/\text{Ni}(\text{OH})_2$	Electrodeposition	1144 Fg^{-1}	5 mVs^{-1}	1 M KOH	6.6 % capacitance decay after 500 cycles	52
Porous Hydroxide nanosheet	Electrodeposition	1095 Fg^{-1}	1 Ag^{-1}	2 M KOH	92% retention after 2000 cycles at 2 Ag^{-1}	22
		812 Fg^{-1}	40 Ag^{-1}			
Co_3O_4 / Activated Carbon	Hydrothermal and calcinations	202 Fg^{-1}	1 Ag^{-1}	6 M KOH	90% retention after 5000 cycles	53
Porous Co_3O_4	Metal Organic Framework followed by thermolysis	150 Fg^{-1}	1 Ag^{-1}	2 M KOH	No capacitance decay after 3400 cycles	46

Co ₃ O ₄ -rGO nanocomposite	Precipitation and thermal treatment	636 Fg ⁻¹	1 Ag ⁻¹	6 M KOH	95% retention after 1000 cycles at 0.625 Ag ⁻¹	1
Nanoporous Co ₃ O ₄	Solvothermal	476 Fg ⁻¹	0.5 Ag ⁻¹	2 M KOH	82% retention after 2000 cycles at 2.5 Ag ⁻¹	25
ZnO @ Co ₃ O ₄ core/shell on Ni form	Hydrothermal	857.7 Fg ⁻¹	1 Ag ⁻¹	2 M KOH	22% Capacitance loss after 6000 cycles 90.1 % and 63.2 % retention for 10000 and 50000 cycles respectively at 40 Ag ⁻¹	54
NiCo ₂ S ₄	Electrodeposition	1418 Fg ⁻¹ 1285 Fg ⁻¹	5 Ag ⁻¹ 100 Ag ⁻¹	1 M KOH		55
Needle like Co ₃ O ₄ anchored on graphene	Hydrothermal	157.7 Fg ⁻¹	0.1 Ag ⁻¹	2 M KOH	70 % retention after 4000 cycles at 0.2 Ag ⁻¹	56
Co ₃ O ₄ NSs-rGO	Hydrothermal	187 Fg ⁻¹	1.2 Ag ⁻¹	2 M KOH	Capacitance loss after 1000 cycles is 11%	47
Hydrous RuO ₂ nanoparticle on Co ₃ O ₄ flakes	Electrodeposition	905 Fg ⁻¹ at	1 Ag ⁻¹	30 wt% KOH	96 % retention after 5000 cycles at 10 Ag ⁻¹	20
Carbon – CoO	Hydrothermal	3282.2 Fg ⁻¹	1 mAcm ⁻²	6 M KOH	96.9% retention after 10000 cycles	13

3D nanonet hollow structure Co ₃ O ₄	Calcination	820 Fg ⁻¹	5 mVs ⁻¹	6 M KOH	90.2 % retention after 1000 cycles at 5 Ag ⁻¹	18
In situ encapsulated Co ₃ O ₄ nanoparticles on carbon nanofiber	Electrospinning	570 Fg ⁻¹	2 Ag ⁻¹	6 M KOH	74 % capacitance retention after 2000 cycles	19
Hierarchical Co ₃ O ₄ /Co(OH) ₂ nanoflakes	Electrodeposition	601 mFcm ⁻²	2 mVs ⁻¹	1 M KOH	92% capacitance retention for optimized sample	21
2D Multilayer graphene like Co ₃ O ₄	Hydrothermal	1752 Fg ⁻¹	5 mVs ⁻¹	6 M KOH	99.5% retention after 2000 cycles at 5 Ag ⁻¹	17
		1862 Fg ⁻¹	1 Ag ⁻¹			
Sub 3-nm Co ₃ O ₄ nanofilms	Hydrothermal	1400 Fg ⁻¹ - Co ₃ O ₄	1 Ag ⁻¹	2 M KOH	Capacitance decayed less than 3% after 1500 cycles	16
		1076 Fg ⁻¹ - Co(OH) ₂				
Co ₃ O ₄ @ CoMoO ₄ core/shell nanowire on Ni form	Hydrothermal Ion Exchange	1040 Fg ⁻¹	1Ag ⁻¹	3 M KOH	12.4% capacitance loss after 5000 cycles	57
Co ₃ O ₄ nanoparticle on Vertically Aligned Graphene	Hydrothermal	3480 Fg ⁻¹	1 mVs ⁻¹	2 M KOH	86.2% capacitance retention after 2000 cycles	14

Co ₃ O ₄ @ MWCNT nanocable	Hydrothermal	590 Fg ⁻¹	15 Ag ⁻¹	0.5 M KOH	No capacitance fading after 2000 cycles	58
		510 Fg ⁻¹	100 Ag ⁻¹			
Co ₃ O ₄ -Polyindole composite	In-situ cathodic electrodeposition	1805 Fg ⁻¹	2 Ag ⁻¹	1 M KOH	82 % capacitance retention	Present Work

Further, Co_3O_4 -Pind composites and pristine Co_3O_4 electrodes are subjected to charge discharge cycling at a current density of 2 Ag^{-1} in the potential range between -0.2 and 0.5 V vs Ag/AgCl . A linear variation of potential with time is observed for both the electrodes as seen in Figure 7(a). The symmetry of the charge and discharge characteristics shows good capacitive behavior⁵⁹. The initial SC values of pristine Co_3O_4 and Co_3O_4 -Pind composites are found to be 1565 and 1805 Fg^{-1} at a current density of 2 Ag^{-1} respectively. This enhanced SC value of Co_3O_4 -Pind composite is mainly attributed to synergistic effect between Co_3O_4 and Pind. Q. Guan et al⁵⁶ have reported needle-like Co_3O_4 anchored on graphene as supercapacitor materials with 157 Fg^{-1} at a current density of 0.1 Ag^{-1} , this value is attributed to the synergism between Co_3O_4 and graphene. However, this SC is much lower than that of Co_3O_4 -Pind composites reported in the present study. Electrospun carbon nanofibers with in Situ encapsulated Co_3O_4 nanoparticles as electrodes for supercapacitors exhibits the SC about 586 Fg^{-1} at a current density of 1 Ag^{-1} .¹⁹ Interestingly, the SC of Co_3O_4 -Pind composite electrodes is three times higher than that of Co_3O_4 /carbon fibers indicating the enhanced supercapacitor behavior of electrodeposited composites materials.

In order to understand the rate capability, the electrodes made from Co_3O_4 -Pind composite were subjected to charge-discharge cycling at different current density values in the range 2 – 25 A g^{-1} . Accordingly, Figure 7 (b) shows the SC of Co_3O_4 -Pind composite as function of different current density values. The SC values of Co_3O_4 -Pind composite are calculated to be 1805 , 1738 , 1700 and 1625 Fg^{-1} at current density values of 2 , 5 , 10 and 25 A g^{-1} respectively. It is clearly seen that there was only a moderate decrease in capacitance (9.9% reduction) when the current density was increased from 2 to 10 mA cm^{-2} . Furthermore, by increasing the current density to 5 times more from 2 Ag^{-1} , more than 94% SC was realized indicating the excellent

rate performance of Co_3O_4 -Pind composite. Interestingly, even at very high current density (25 Ag^{-1}) the SC of Co_3O_4 -Pind composite is found to be 1625 Fg^{-1} which is almost 90 % of the initial SC obtained at 2 Ag^{-1} . However, further increase in current density decreases the SC due to a decrease in the efficiency of utilization of the active material at high current density values.⁶⁰⁻⁶² Various nanostructures Co_3O_4 and its composites synthesized by different methods have been reported as the electrode materials for supercapacitors as shown in Table 1. Compared with the reported results, the Co_3O_4 -Pind composite exhibits superior electrochemical performance attributed to its distinctive structures of Co_3O_4 and synergism between oxides and Pind facilitating electron transportation and ion diffusion during the charge-discharge process.

The electrochemical behaviour of pristine Co_3O_4 and Co_3O_4 -Pind composites was also studied using electrochemical impedance spectroscopy frequency intercept on the real axis corresponding to ohmic resistance arises due to the electrolyte, current collection, current leads, etc. and the broad semicircle arises due to parallel combination of charge-transfer resistance (R_{ct}) and double layer capacitance (C_{dl}) with a linear region at low frequency range. It is known that low frequency linear plot of impedance is found to be 45° to the real axis if the process is governed by diffusion controlled process or it should make 90° if the behavior is purely capacitive in nature. Here, the ohmic resistance of all three electrodes is found to be similar (Ω) indicating the common electrolyte used for all the electrochemical measurements. However, there is a variation in the charge-transfer resistance among the electrodes. It is clear from Nyquist plot (Figure 4) that the charge transfer resistance of Cobalt oxide is much higher in the range between 100 mHz to 1 MHz with respect to open circuit potential. Nyquist and Bode plots of A.C impedance spectra of all electrodes are shown in Figure 8. The bode plots of phase angle vs $\log(f)$ gave phase angle shift. The Co_3O_4 -Pind behaves typical capacitive characteristic at low

frequency and impedance characteristic at high frequency, which is quite different from that of the Co_3O_4 and Pind. At zero frequency region (0.16 Hz), Co_3O_4 -Pind and Pind having the higher phase angle compare with Co_3O_4 . The deviations of phase angle from 90° facilitate the pseudo capacitive behaviour. Co_3O_4 -Pind having better charge accumulation material compare with Pind and Co_3O_4 . Nyquist plot (Figure 8) consists of a high than that of composition and pristine Pind. The lower R_{ct} value of Co_3O_4 -Pind is due to the anchoring Pind on oxide matrix.

The cycle life test was performed for Co_3O_4 -Pind composites at a current density of 25 Ag^{-1} and the corresponding data is shown in Figure 9. The initial SC of Co_3O_4 -Pind composites electrode is found to be 1600 Fg^{-1} . The Co_3O_4 -Pind electrode retains the SC of 1417 and 1342 Fg^{-1} after 200 and 600 cycles respectively. Similarly, after 800 cycles, the SC of Co_3O_4 -Pind electrode is obtained as 1333 Fg^{-1} . However, there is a large decay in SC in pristine Co_3O_4 compared to composites electrodes. Further, the SC of Co_3O_4 -Pind composite electrode after 1000 cycles was found to be about 1358 F g^{-1} which is 85 % of the initial capacitance. However, the pristine Co_3O_4 exhibits only 67% SC is retained initial SC indicating the significant impact of the composites electrodes in supercapacitors.

Conclusions

In summary, we have successfully demonstrated the single step synthesis of Co_3O_4 -Pind composite using *in-situ* cathodic polymerization. All physicochemical characterization clearly indicates the existence of spinel structure of Co_3O_4 anchored by Pind. More importantly, the Co_3O_4 -Pind composite electrode offers enhanced SC, excellent rate capability (1805 and 1625 Fg^{-1} at 2 and 25 Ag^{-1} respectively) and cycling stability. This remarkable supercapacitive behaviour is mainly attributed to the synergetic effect raised between Co_3O_4 and Pind.

Furthermore, this simple synthetic strategy opens up new avenue to prepare various other metal oxides and polymers for energy applications.

Acknowledgements

Pavul Raj thanks UGC for providing financial support. Ragupathy recognizes the DST, India for financial assistance through SERC Fast Track Scheme no. SR/FT/CS-74/2011. Authors also acknowledge Dr. Vijayamohanan K. Pillai, Director, CSIR-CECRI for their continuous support and constant encouragement.

References:

- (1) Xie, L.-J.; Wu, J.-F.; Chen, C.-M.; Zhang, C.-M.; Wan, L.; Wang, J.-L.; Kong, Q.-Q.; Lv, C.-X.; Li, K.-X.; Sun, G.-H. A Novel Asymmetric Supercapacitor with an Activated Carbon Cathode and a Reduced Graphene Oxide–cobalt Oxide Nanocomposite Anode. *J. Power Sources* **2013**, *242*, 148–156.
- (2) Zhang, Q.; Uchaker, E.; Candelaria, S. L.; Cao, G. Nanomaterials for Energy Conversion and Storage. *Chem. Soc. Rev.* **2013**, *42* (7), 3127–3171.
- (3) Xie, K.; Wei, B. Materials and Structures for Stretchable Energy Storage and Conversion Devices. *Adv. Mater.* **2014**, *26* (22), 3592–3617.
- (4) Simon, P.; Gogotsi, Y. Materials for Electrochemical Capacitors. *Nat. Mater.* **2008**, *7* (11), 845–854.
- (5) Xiang, C.; Li, M.; Zhi, M.; Manivannan, A.; Wu, N. A Reduced Graphene oxide/Co₃O₄ Composite for Supercapacitor Electrode. *J. Power Sources* **2013**, *226*, 65–70.
- (6) Soc, C.; Wang, G.; Zhang, J. A Review of Electrode Materials for Electrochemical Supercapacitors. *Chem. Soc. Rev.* **2012**, *41*, 797–828.
- (7) Naoi, K.; Simon, P. New Materials and New Configurations for Advanced Electrochemical Capacitors. *J. Electrochem. Soc.* **2008**, *17* (1), 34–37.
- (8) Rolison, D. R.; Long, J. W.; Lytle, J. C.; Fischer, A. E.; Rhodes, C. P.; McEvoy, T. M.; Bourg, M. E.; Lubers, A. M. Multifunctional 3D Nanoarchitectures for Energy Storage and Conversion. *Chem. Soc. Rev.* **2009**, *38* (1), 226–252.
- (9) Morita, M. Advanced Polymers as Active Materials and Electrolytes for Electrochemical Capacitors and Hybrid Capacitor Systems. *J. Electrochem. Soc.* **2008**, *17* (1), 44–48.
- (10) Zheng, J. P. Hydrous Ruthenium Oxide as an Electrode Material for Electrochemical Capacitors. *J. Electrochem. Soc.* **1995**, *142* (8), 2699.
- (11) Farhadi, S.; Safabakhsh, J.; Zaringhadam, P. Synthesis, Characterization, and

- Investigation of Optical and Magnetic Properties of Cobalt Oxide (Co₃O₄) Nanoparticles. *J. Nanostructure Chem.* **2013**, 3 (1), 69.
- (12) Lokhande, C. D.; Dubal, D. P.; Joo, O.-S. Metal Oxide Thin Film Based Supercapacitors. *Curr. Appl. Phys.* **2011**, 11 (3), 255–270.
- (13) Wang, H.; Qing, C.; Guo, J.; Aref, A. A.; Sun, D.; Wang, B.; Tang, Y. Highly Conductive carbon–CoO Hybrid Nanostructure Arrays with Enhanced Electrochemical Performance for Asymmetric Supercapacitors. *J. Mater. Chem. A* **2014**, 2 (30), 11776.
- (14) Liao, Q.; Li, N.; Jin, S.; Yang, G.; Wang, C. All-Solid-State Symmetric Supercapacitor Based on Co₃O₄ Nanoparticles on Vertically Aligned Graphene. *ACS Nano* **2015**, 9 (5), 5310–5317.
- (15) Gu, Z.; Wang, R.; Nan, H.; Geng, B.; Zhang, X. Construction of Unique Co₃O₄@CoMoO₄ Core/shell Nanowire Arrays on Ni Foam by the Action Exchange Method for High-Performance Supercapacitors. *J. Mater. Chem. A* **2015**, 3 (28), 14578–14584.
- (16) Feng, C.; Zhang, J.; He, Y.; Zhong, C.; Hu, W.; Liu, L.; Deng, Y. Sub-3 Nm Co₃O₄ Nanofilms with Enhanced Supercapacitor Properties. *ACS Nano* **2015**, 9 (2), 1730–1739.
- (17) Xuan, L.; Chen, L.; Yang, Q.; Chen, W.; Hou, X.; Jiang, Y.; Zhang, Q.; Yuan, Y. Engineering 2D Multi-Layer Graphene-like Co₃O₄ Thin Sheets with Vertically Aligned Nanosheets as Basic Building Units for Advanced Pseudocapacitor Materials. *J. Mater. Chem. A* **2015**.
- (18) Wang, Y.; Lei, Y.; Li, J.; Gu, L.; Yuan, H.; Xiao, D. Synthesis of 3D-Nanonet Hollow Structured Co₃O₄ for High Capacity Supercapacitor. *ACS Appl. Mater. Interfaces* **2014**, 6 (9), 6739–6747.
- (19) Abouali, S.; Akbari Garakani, M.; Zhang, B.; Xu, Z.-L.; Kamali Heidari, E.; Huang, J.-Q.; Huang, J.; Kim, J.-K. Electrospun Carbon Nanofibers with in Situ Encapsulated Co₃O₄ Nanoparticles as Electrodes for High-Performance Supercapacitors. *ACS Appl. Mater. Interfaces* **2015**, 7 (24), 13503–13511.
- (20) Rakhi, R. B.; Chen, W.; Hedhili, M. N.; Cha, D.; Alshareef, H. N. Enhanced Rate Performance of Mesoporous Co(3)O(4) Nanosheet Supercapacitor Electrodes by Hydrous RuO(2) Nanoparticle Decoration. *ACS Appl. Mater. Interfaces* **2014**, 6 (6), 4196–4206.

- (21) Qorbani, M.; Naseri, N.; Moshfegh, A. Z. Hierarchical Co₃O₄/Co(OH)₂ Nanoflakes as a Supercapacitor Electrode: Experimental and Semi-Empirical Model. *ACS Appl. Mater. Interfaces* **2015**, *7* (21), 11172–11179.
- (22) Xia, X.; Tu, J.; Zhang, Y.; Chen, J.; Wang, X.; Gu, C.; Guan, C.; Luo, J.; Fan, H. J. Porous Hydroxide Nanosheets on Preformed Nanowires by Electrodeposition: Branched Nanoarrays for Electrochemical Energy Storage. *Chem. Mater.* **2012**, *24* (19), 3793–3799.
- (23) Kung, C.-W.; Chen, H.-W.; Lin, C.-Y.; Vittal, R.; Ho, K.-C. Synthesis of Co₃O₄ Nanosheets via Electrodeposition Followed by Ozone Treatment and Their Application to High-Performance Supercapacitors. *J. Power Sources* **2012**, *214*, 91–99.
- (24) Meher, S. K.; Rao, G. R. Ultralayered Co₃O₄ for High-Performance Supercapacitor Applications. *J. Phys. Chem. C* **2011**, *115* (31), 15646–15654.
- (25) Deori, K.; Ujjain, S. K.; Sharma, R. K.; Deka, S. Morphology Controlled Synthesis of Nanoporous Co₃O₄ Nanostructures and Their Charge Storage Characteristics in Supercapacitors. *ACS Appl. Mater. Interfaces* **2013**, *5*, 10665–10672.
- (26) Yang, D. Application of Nanocomposites for Supercapacitors: Characteristics and Properties. In *Nanocomposites - New Trends and Developments*; Ebrahimi, F., Ed.; InTech, 2012; pp 299–328.
- (27) He, G.; Li, J.; Chen, H.; Shi, J.; Sun, X.; Chen, S.; Wang, X. Hydrothermal Preparation of Co₃O₄@graphene Nanocomposite for Supercapacitor with Enhanced Capacitive Performance. *Mater. Lett.* **2012**, *82*, 61–63.
- (28) Shan, Y.; Gao, L. Formation and Characterization of Multi-Walled Carbon nanotubes/Co₃O₄ Nanocomposites for Supercapacitors. *Mater. Chem. Phys.* **2007**, *103* (2-3), 206–210.
- (29) Snook, G. A.; Kao, P.; Best, A. S. Conducting-Polymer-Based Supercapacitor Devices and Electrodes. *J. Power Sources* **2011**, *196* (1), 1–12.
- (30) Kumar, A.; Pandey, A. C.; Prakash, R. Electro-Oxidation of Formic Acid Using Polyindole-SnO₂ Nanocomposite. *Catal. Sci. Technol.* **2012**, *2* (12), 2533.
- (31) Trung, V. Q.; Huyen, D. N. Synthesis, Properties and Application of polyindole/TiO₂ Nanocomposites. *J. Phys. Conf. Ser.* **2009**, *187* (1), 012058.

- (32) Jung, Y.; Singh, N.; Choi, K.-S. Cathodic Deposition of Polypyrrole Enabling the One-Step Assembly of Metal-Polymer Hybrid Electrodes. *Angew. Chem. Int. Ed. Engl.* **2009**, *48* (44), 8331–8334.
- (33) Jung, Y.; Spray, R. L.; Kim, J. H.; Kim, J. M.; Choi, K.-S. Selective Polymerization of Polypyrrole in Silica Mesopores Using an in Situ Generated Oxidizing Agent on a Silica Surface. *Chem. Commun. (Camb)*. **2010**, *46* (35), 6566–6568.
- (34) Koh, J. Y.; Jung, Y. Nanoscale Morphology Control of Conducting Polymers by Cathodic Polymerization Route. *Int. J. Electrochem. Sci.* **2013**, *8* (7), 10080–10085.
- (35) McKeown, D. A. Raman Spectroscopy and Vibrational Analyses of Albite: From 25 C through the Melting Temperature. *Am. Mineral.* **2005**, *90* (10), 1506–1517.
- (36) Raveau, B.; Seikh, M. M. Crystal Chemistry of Cobalt Oxides. In *Cobalt Oxides: From Crystal Chemistry to Physics*; Raveau, B., Seikh, M. M., Eds.; Wiley-VCH Verlag GmbH & Co. KGaA: Weinheim, Germany, 2012; pp 3–70.
- (37) Nam, D.-H.; Lim, S.-J.; Kim, M.-J.; Kwon, H.-S. Facile Synthesis of SnO₂-Polypyrrole Hybrid Nanowires by Cathodic Electrodeposition and Their Application to Li-Ion Battery Anodes. *RSC Adv.* **2013**, *3* (36), 16102.
- (38) Roy, R.; White, W. B. Infrared Spectra-Crystal Structure Correlations: II. Comparison of Simple Polymorphic Minerals. *Am. Mineral.* **1964**, *49* (11-12), 1670–1687.
- (39) Taylan, N. B.; Sari, B.; Unal, H. I. Preparation of Conducting Poly (Vinyl Chloride)/ Polyindole Composites and Freestanding Films via Chemical Polymerization. *J. Polym. Sci. Part B Polym. Phys.* **2010**, *48* (March), 1290–1298.
- (40) Rajasudha, G.; Nancy, a. P.; Paramasivam, T.; Boukos, N.; Narayanan, V.; Stephen, a. Synthesis and Characterization of Polyindole–NiO-Based Composite Polymer Electrolyte with LiClO₄. *Int. J. Polym. Mater.* **2011**, *60* (11), 877–892.
- (41) Domínguez, M.; Taboada, E.; Idriss, H.; Molins, E.; Llorca, J. Fast and Efficient Hydrogen Generation Catalyzed by Cobalt Talc Nanolayers Dispersed in Silica Aerogel. *J. Mater. Chem.* **2010**, *20* (23), 4875.

- (42) Yue, J.; Epstein, J. Xps Study of Self-Doped Conducting Polyaniline and Parent Systems. *Macromolecules* **1991**, *24* (15), 4441–4445.
- (43) Dwivedi, N.; Yeo, R. J.; Satyanarayana, N.; Kundu, S.; Tripathy, S.; Bhatia, C. S. Understanding the Role of Nitrogen in Plasma-Assisted Surface Modification of Magnetic Recording Media with and without Ultrathin Carbon Overcoats. *Sci. Rep.* **2015**, *5*, 7772.
- (44) Hua, M. Y.; Chen, C. J.; Chen, H. C.; Tsai, R. Y.; Cheng, W.; Cheng, C. L.; Liu, Y. C. Preparation of a Porous Composite Film for the Fabrication of a Hydrogen Peroxide Sensor. *Sensors* **2011**, *11* (6), 5873–5885.
- (45) Deniau, G.; Azoulay, L.; Jégou, P.; Le Chevallier, G.; Palacin, S. Carbon-to-Metal Bonds: Electrochemical Reduction of 2-Butenenitrile. *Surf. Sci.* **2006**, *600* (3), 675–684.
- (46) Meng, F. L.; Fang, Z. G.; Li, Z. X.; Xu, W. W.; Wang, M. J.; Liu, Y. P.; Zhang, J.; Wang, W. R.; Zhao, D. Y.; Guo, X. H. Porous Co₃O₄ Materials Prepared by Solid-State Thermolysis of a Novel Co-MOF Crystal and Their Superior Energy Storage Performances for Supercapacitors. *J. Mater. Chem. A* **2013**, *1* (24), 7235–7241.
- (47) Yuan, C.; Zhang, L.; Hou, L.; Pang, G.; Oh, W.-C. One-Step Hydrothermal Fabrication of Strongly Coupled Co₃O₄ Nanosheets–reduced Graphene Oxide for Electrochemical Capacitors. *RSC Adv.* **2014**, *4* (28), 14408.
- (48) Zhang, G.; Wang, T.; Yu, X.; Zhang, H.; Duan, H.; Lu, B. Nanoforest of Hierarchical Co₃O₄@NiCo₂O₄ Nanowire Arrays for High-Performance Supercapacitors. *Nano Energy* **2013**, *2* (5), 586–594.
- (49) Casella, I. G.; Gatta, M. Study of the Electrochemical Deposition and Properties of Cobalt Oxide Species in Citrate Alkaline Solutions. *J. Electroanal. Chem.* **2002**, *534* (1), 31–38.
- (50) Kandalkar, S. G.; Lee, H.; Chae, H.; Kim, C. Structural, Morphological, and Electrical Characteristics of the Electrodeposited Cobalt Oxide Electrode for Supercapacitor Applications. *Mater. Res. Bull.* **2011**, *46* (1), 48–51.
- (51) Yuan, Y. F.; Xia, X. H.; Wu, J. B.; Huang, X. H.; Pei, Y. B.; Yang, J. L.; Guo, S. Y. Hierarchically Porous Co₃O₄ with Mesoporous Walls Prepared via Liquid Crystalline Template for Supercapacitor Application. *Electrochem. commun.* **2011**, *13* (3), 1123–1126.

- (52) Zhong, J.-H.; Wang, A.-L.; Li, G.-R.; Wang, J.-W.; Ou, Y.-N.; Tong, Y.-X. Co₃O₄/Ni(OH)₂ Composite Mesoporous Nanosheet Networks as a Promising Electrode for Supercapacitor Applications. *J. Mater. Chem.* **2012**, *22* (12), 5656.
- (53) Zhang, C.; Xie, L.; Song, W.; Wang, J.; Sun, G.; Li, K. Electrochemical Performance of Asymmetric Supercapacitor Based on Co₃O₄ / AC Materials. *J. Electroanal. Chem.* **2013**, *706*, 1–6.
- (54) Cai, D.; Huang, H.; Wang, D.; Liu, B.; Wang, L.; Liu, Y.; Li, Q.; Wang, T. High-Performance Supercapacitor Electrode Based on the Unique ZnO @ Co₃O₄ Core / Shell Heterostructures on Nickel Foam. *ACS Appl. Mater. Interfaces* **2014**, *6*, 15905–15912.
- (55) Chen, W.; Xia, C.; Alshareef, H. N. One-Step Electrodeposited Nickel Cobalt Sulfide Nanosheet Arrays for High-Performance Asymmetric Supercapacitors. *ACS Nano* **2014**, *8* (9), 9531–9541.
- (56) Guan, Q.; Cheng, J.; Wang, B.; Ni, W.; Gu, G.; Li, X.; Huang, L.; Yang, G.; Nie, F. Needle-like Co₃O₄ Anchored on the Graphene with Enhanced Electrochemical Performance for Aqueous Supercapacitors. *ACS Appl. Mater. Interfaces* **2014**, *6*, 7626–7632.
- (57) Zhang, X. Construction of Unique Co₃O₄@CoMoO₄ Core/shell Nanowire Arrays on Ni Foam by the Action Exchange Method for High-Performance Supercapacitors. *J. Mater. Chem. A Mater. energy Sustain.* **2015**, *3* (28), 14578–14584.
- (58) Wang, X.; Li, M.; Chang, Z.; Yang, Y.; Wu, Y.; Liu, X. Co₃O₄@MWCNT Nanocable as Cathode with Superior Electrochemical Performance for Supercapacitors. *ACS Appl. Mater. Interfaces* **2015**, *7*, 2280–2285.
- (59) Estaline Amitha, F.; Leela Mohana Reddy, A.; Ramaprabhu, S. A Non-Aqueous Electrolyte-Based Asymmetric Supercapacitor with Polymer and Metal Oxide/multiwalled Carbon Nanotube Electrodes. *J. Nanoparticle Res.* **2008**, *11* (3), 725–729.
- (60) Munaiah, Y.; Sundara Raj, B. G.; Prem Kumar, T.; Ragupathy, P. Facile Synthesis of Hollow Sphere Amorphous MnO₂: The Formation Mechanism, Morphology and Effect of a Bivalent Cation-Containing Electrolyte on Its Supercapacitive Behavior. *J. Mater. Chem. A* **2013**, *1* (13), 4300.
- (61) Ragupathy, P.; Vasana, H. N.; Munichandraiah, N. Synthesis and Characterization of

- Nano-MnO₂ for Electrochemical Supercapacitor Studies. *J. Electrochem. Soc.* **2008**, *155* (1), A34.
- (62) Ragupathy, P.; Park, D. H.; Campet, G.; Vasan, H. N.; Hwang, S. J.; Choy, J. H.; Munichandraiah, N. Remarkable Capacity Retention of Nanostructured Manganese Oxide upon Cycling as an Electrode Material for Supercapacitor. *J. Phys. Chem. C* **2009**, *113* (15), 6303–6309.

Figure Captions:

1. X-ray diffraction pattern of (i) pristine Co_3O_4 and (ii) Co_3O_4 -Pind composites.
2. (a) Laser Raman Spectra of (i) pristine Co_3O_4 (ii) Co_3O_4 -Pind and (iii) Pind and (b) FTIR graphs of prepared (i) pristine Co_3O_4 and (ii) Co_3O_4 -Pind composites.
3. XPS spectra of Co_3O_4 -Pind composite (a) Co_{2p} (b) C_{1s} (c) N_{1s} and (d) O_{1s} .
4. SEM images of prepared (a) pristine Co_3O_4 (b) Co_3O_4 -Pind (c) Pind and the inset images correspond to EDX spectra.
5. TEM image of Co_3O_4 -Pind (a) and corresponding SAED pattern (b).
6. (a) Cyclic voltammograms of (i) pristine Co_3O_4 (ii) Co_3O_4 -Pind and (iii) Pind at 5 mVs^{-1} in 1 M KOH (b) various scan rate at (i) 1 (ii) 5 (iii) 10 (iv) 25 (v) 50 (vi) 75 and (vii) 100 mVs^{-1} .
7. (a) Galvanostatic charge – discharge graphs of (i) Co_3O_4 -Pind (ii) Co_3O_4 and (b) rate capacitance graphs for (i) Co_3O_4 -Pind and (ii) pristine Co_3O_4 .
8. (a) Electrochemical impedance spectrum as Nyquist plot and (b) Bode plot for (i) Co_3O_4 (ii) Co_3O_4 -Pind and (iii) Pind.
9. Cycle life test of (i) Co_3O_4 -Pind composite and (ii) pristine Co_3O_4 .

Schematic illustrations of high performance Supercapacitor behaviour of Co_3O_4 -Pind composites.

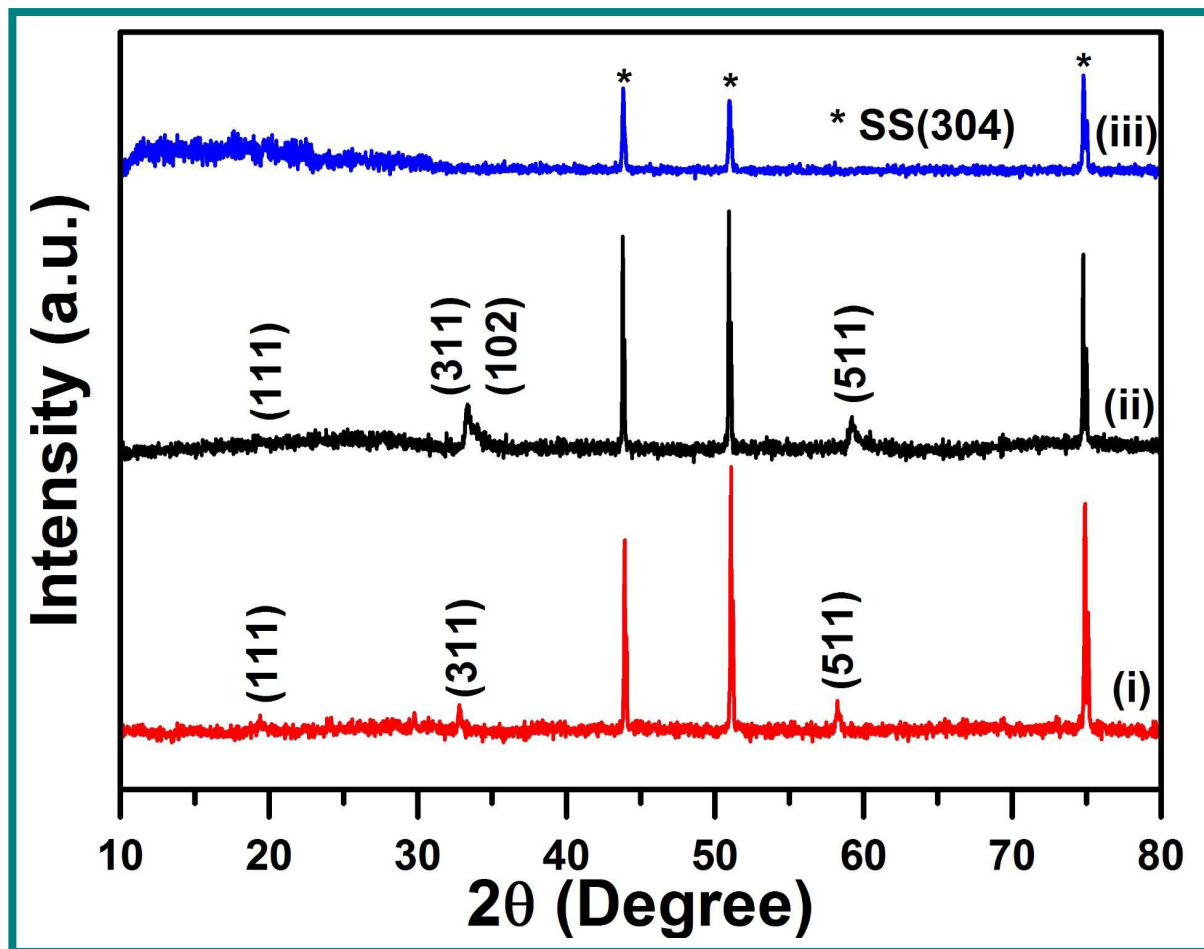


Figure 1

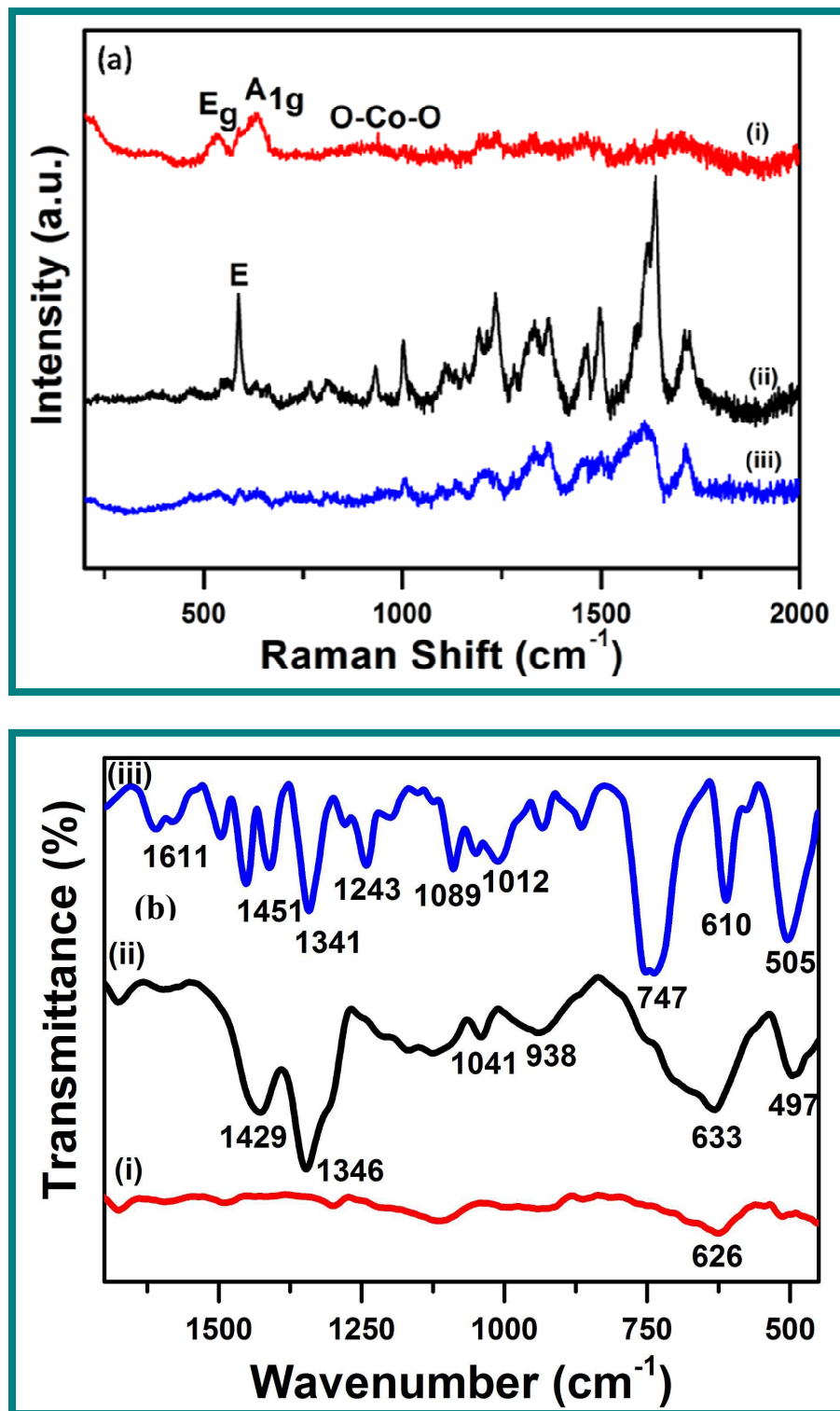
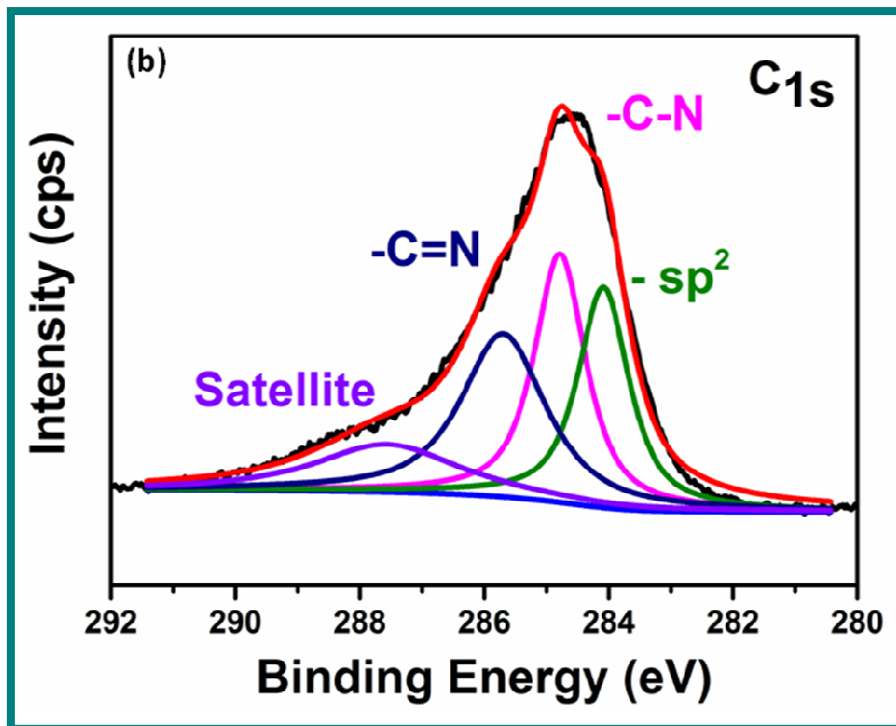
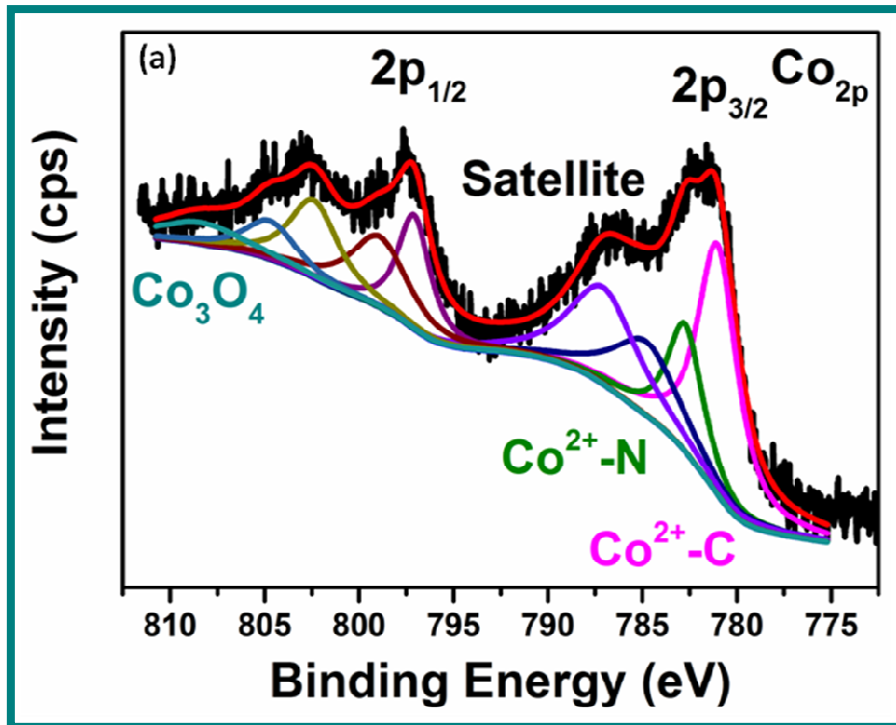


Figure 2



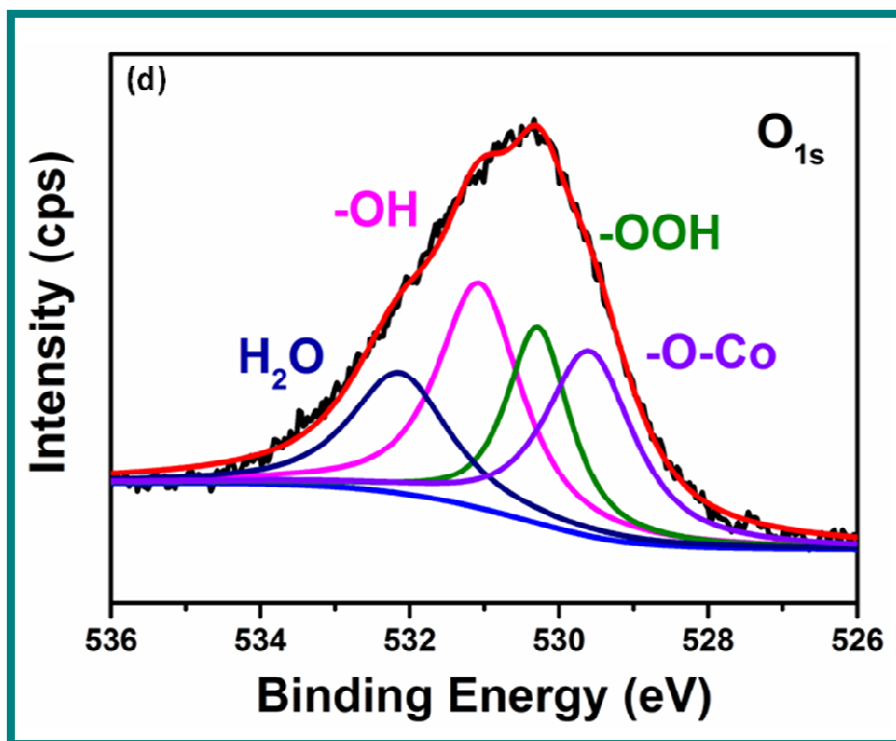
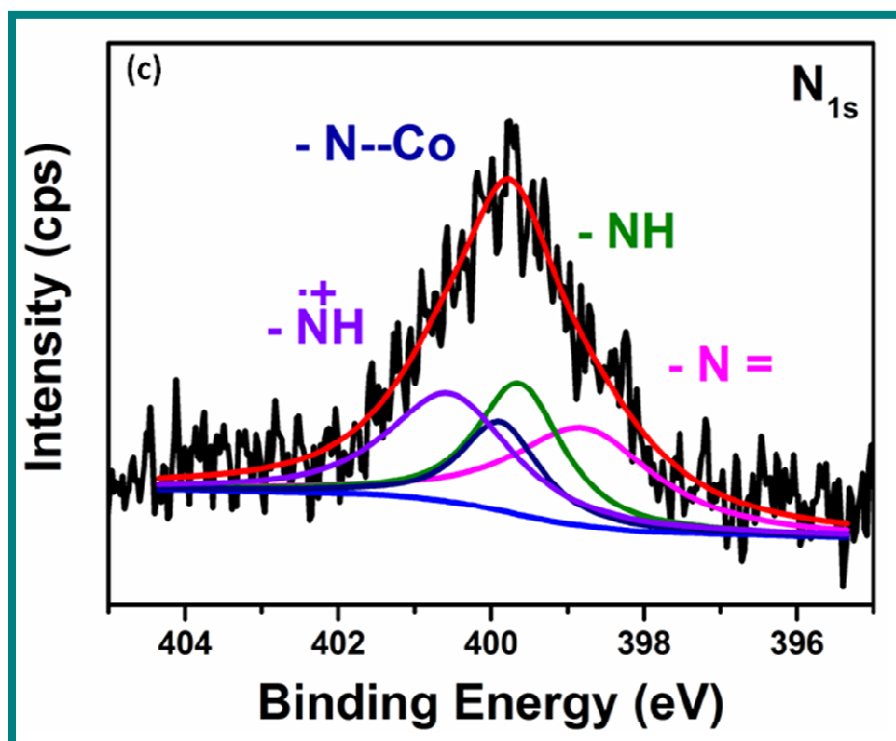


Figure 3

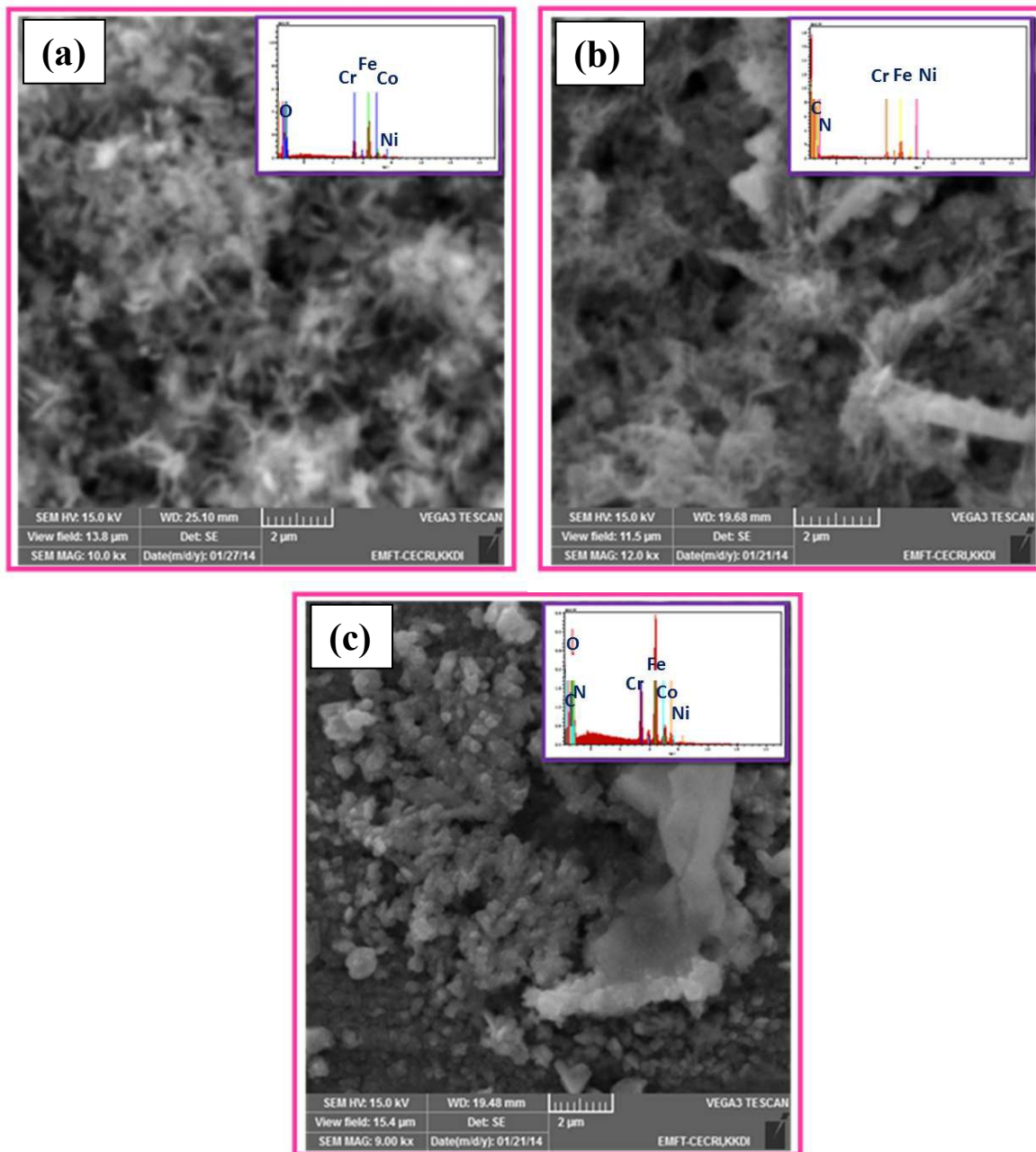


Figure 4

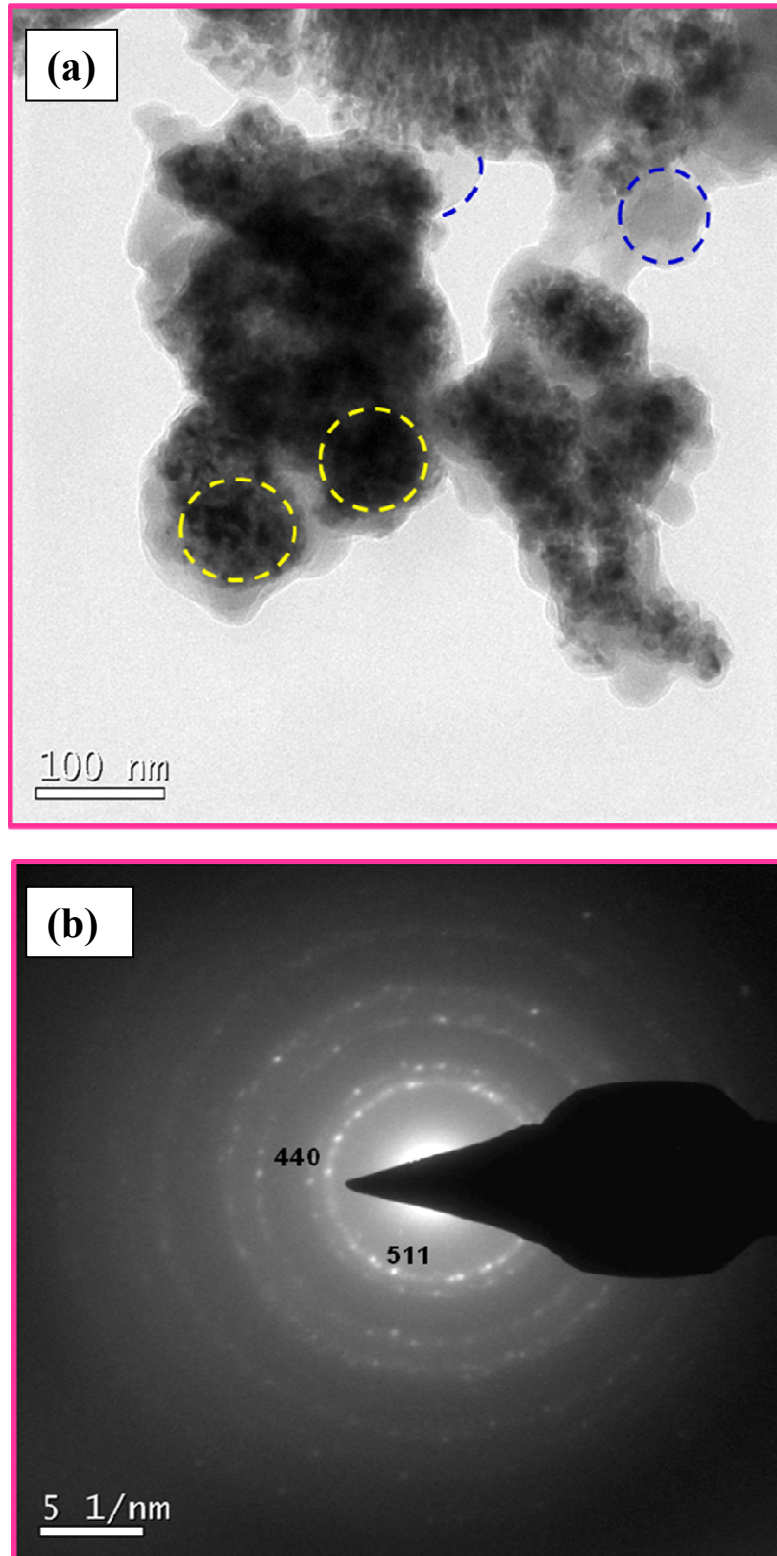


Figure 5

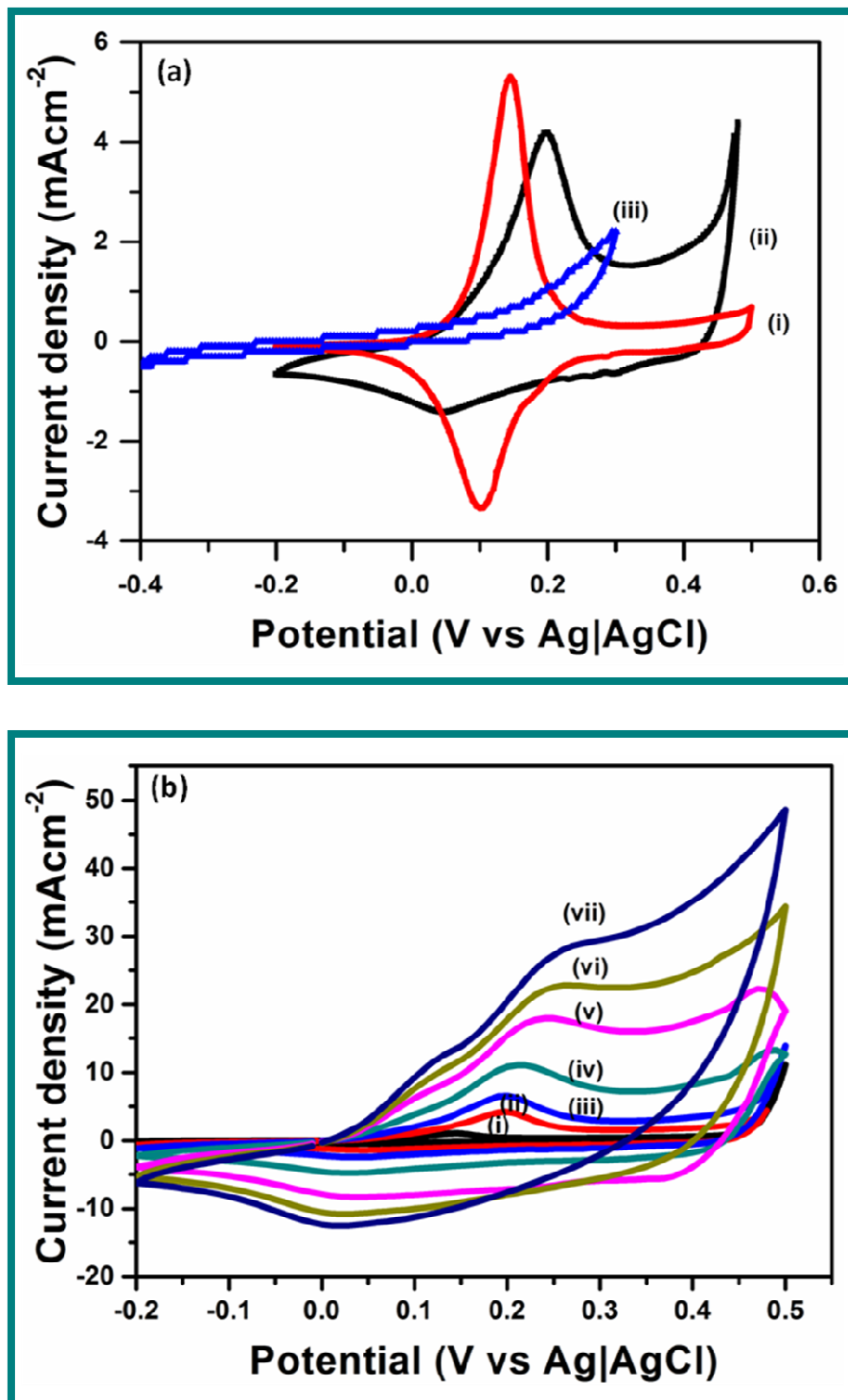


Figure 6

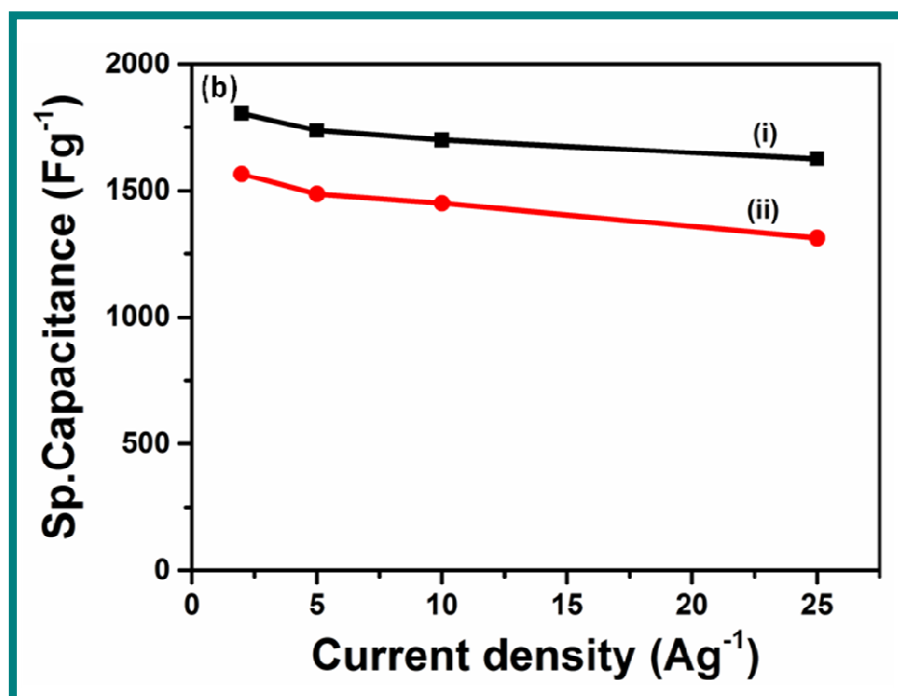
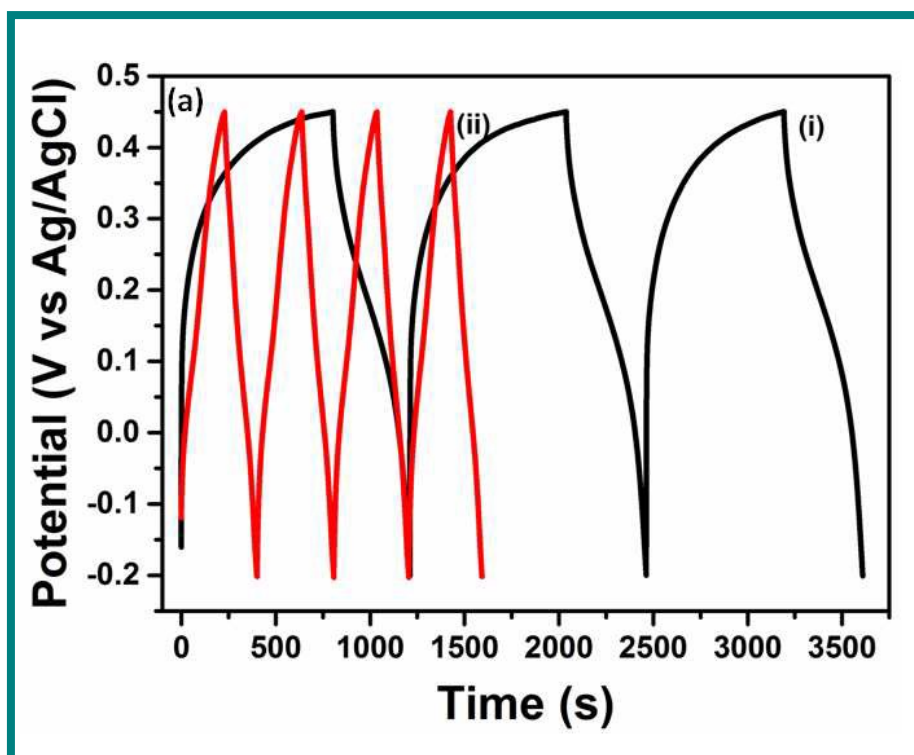


Figure 7

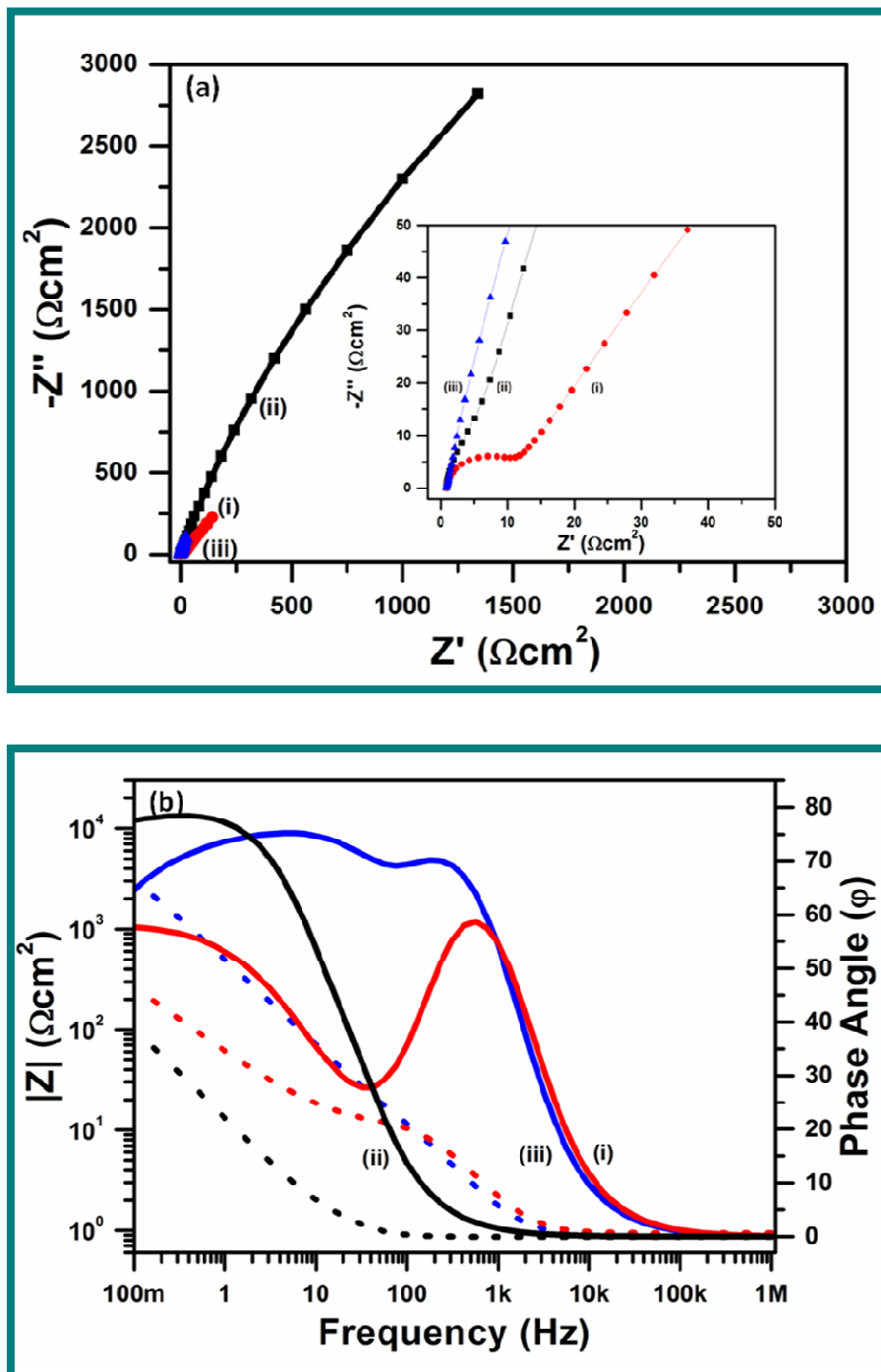


Figure 8

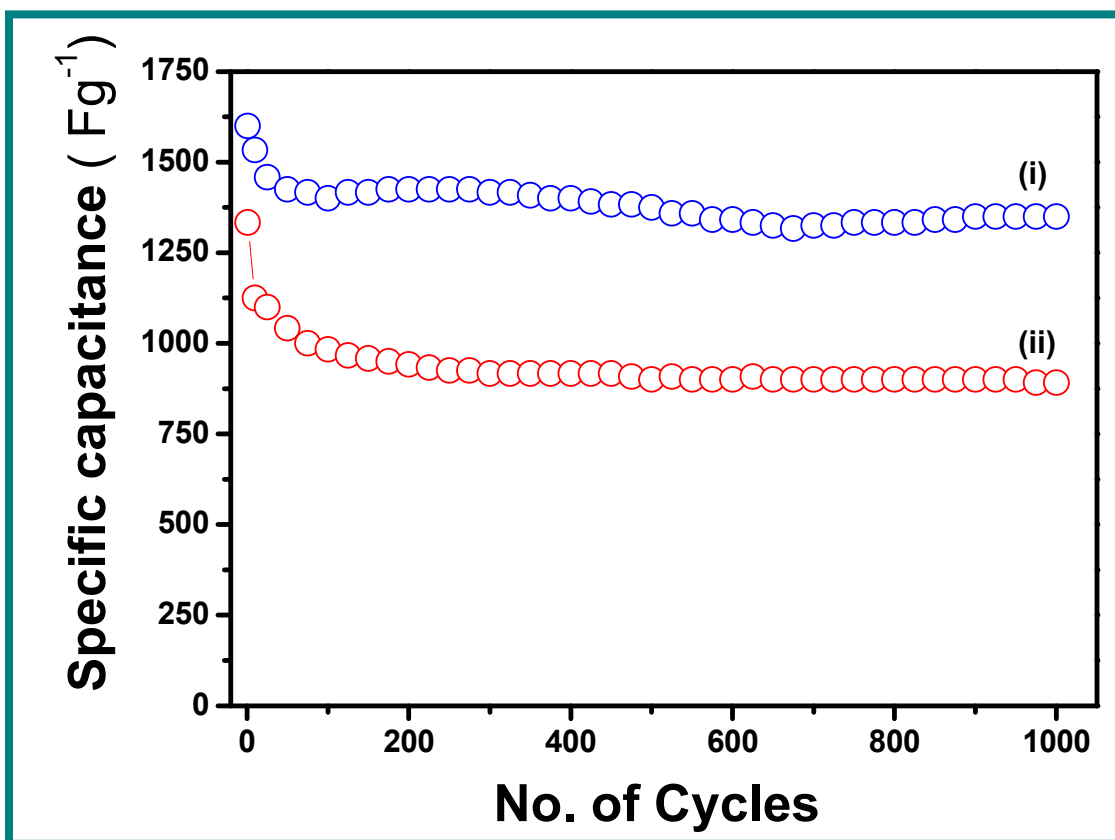
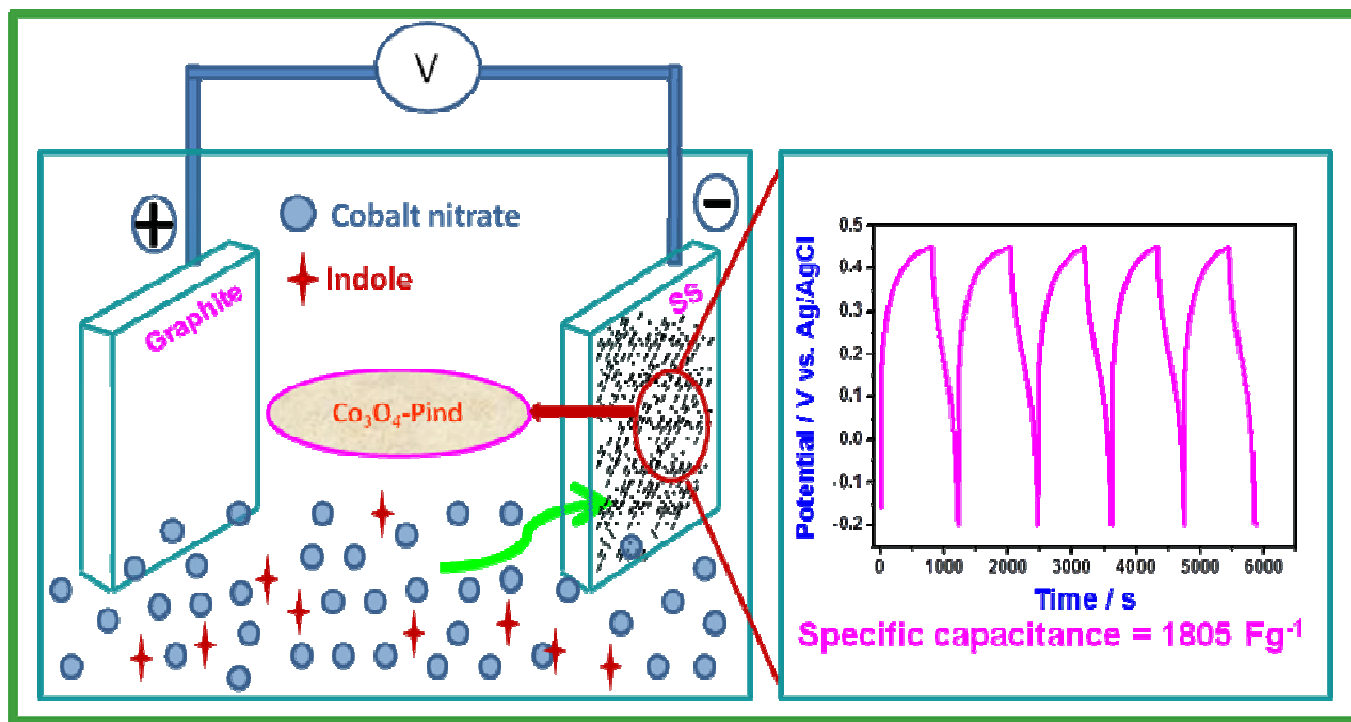


Figure 9

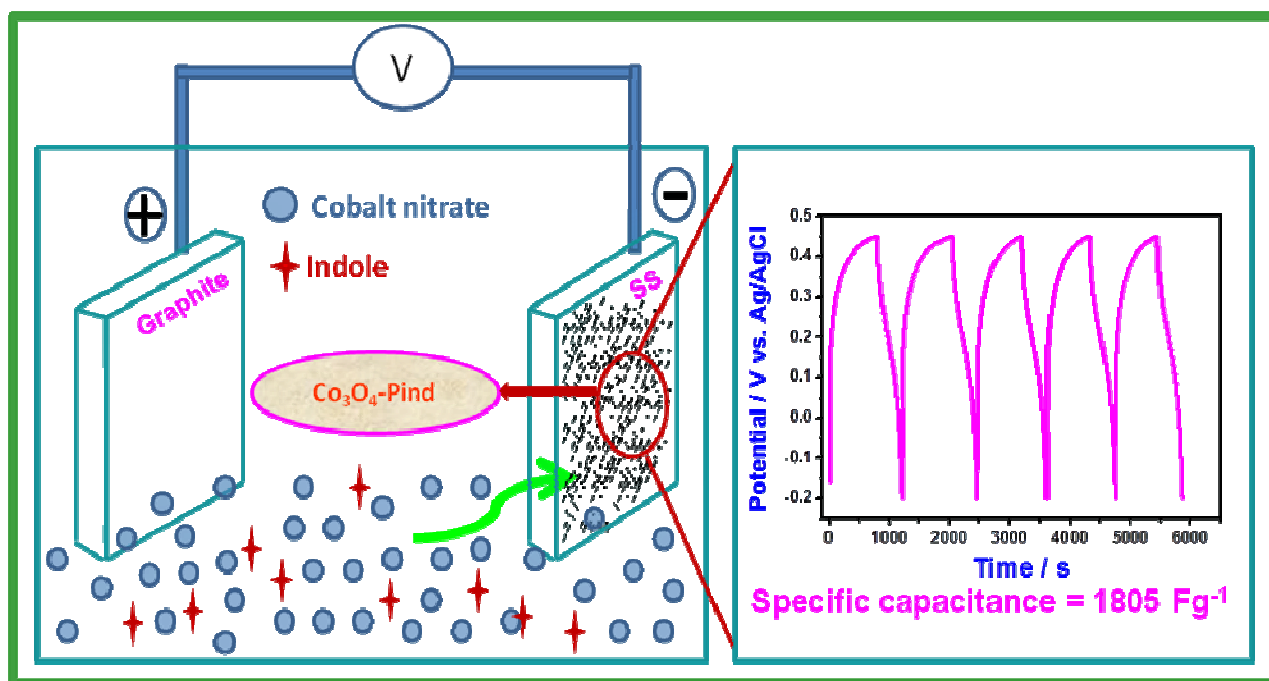


Scheme

Graphical content:**Remarkable Capacitive Behavior of Co_3O_4 -Polyindole Composite as Electrode Material for Supercapacitor Applications**

*R. Pavul Raj, P. Ragupathy, S. Mohan**

A single step synthesized Co_3O_4 -Polyindole composite electrode exhibits high the specific capacitance, rate performance and cyclability. This enhanced electrochemical supercapacitive behavior is mainly attributed to the synergistic effect between Co_3O_4 and Polyindole.



Keywords: synergetic effect; Co_3O_4 -Polyindole; energy storage; composites electrodes